Chinese Journal of Catalysis 37 (2016) 539–548

available at www.sciencedirect.com

ScienceDirect

journal homepage: www.elsevier.com/locate/chnjc

Article

# A Fe-N-C catalyst with highly dispersed iron in carbon for oxygen reduction reaction and its application in direct methanol fuel cells

Lingzheng Gu [a,c], Luhua Jiang [a,*], Xuning Li [b,c], Jutao Jin [a], Junhu Wang [b], Gongquan Sun [a,#]

[a] *Division of Fuel Cell & Battery, Dalian National Laboratory for Clean Energy, Dalian Institute of Chemical Physics, Chinese Academy of Sciences, Dalian 116023, Liaoning, China*

[b] *Mössbauer Effect Data Center, Dalian Institute of Chemical Physics, Chinese Academy of Sciences, Dalian 116023, Liaoning, China*

[c] *University of Chinese Academy of Sciences, Beijing 100049, China*

ARTICLE INFO

*Article history:*
Received 7 January 2016
Accepted 29 January 2016
Published 5 April 2016

*Keywords:*
Highly dispersed iron
Microporous carbon
Oxygen reduction reaction
Direct methanol fuel cell

ABSTRACT

Exploring non-precious metal catalysts for the oxygen reduction reaction (ORR) is essential for fuel cells and metal–air batteries. Herein, we report a Fe-N-C catalyst possessing a high specific surface area (1501 $m^2/g$) and uniformly dispersed iron within a carbon matrix prepared *via* a two-step pyrolysis process. The Fe-N-C catalyst exhibits excellent ORR activity in 0.1 mol/L NaOH electrolyte (onset potential, $E_o$ = 1.08 V and half wave potential, $E_{1/2}$ = 0.88 V vs. reversible hydrogen electrode) and 0.1 mol/L $HClO_4$ electrolyte ($E_o$ = 0.85 V and $E_{1/2}$ = 0.75 V vs. reversible hydrogen electrode). The direct methanol fuel cells employing Fe-N-C as the cathodic catalyst displayed promising performance with a maximum power density of 33 $mW/cm^2$ in alkaline media and 47 $mW/cm^2$ in acidic media. The detailed investigation on the composition–structure–performance relationship by X-ray diffraction, X-ray photoelectron spectroscopy and Mössbauer spectroscopy suggests that Fe-$N_4$, together with graphitic-N and pyridinic-N are the active ORR components. The promising direct methanol fuel cell performance displayed by the Fe-N-C catalyst is related to the intrinsic high catalytic activity, and critically for this application, to the high methanol tolerance.



## 1. Introduction

The oxygen reduction reaction (ORR) is the cathodic reaction of energy sources such as fuel cells and metal–air batteries. The slow kinetics of the ORR hinders the performance of such energy-related technologies. Presently, Pt and its alloys set the benchmark for ORR, being the most active catalysts, however, the limited reserves and the high cost of Pt limits commercialization of the above power sources. The pursuit of highly efficient and low-cost electrocatalysts to replace current expensive Pt catalysts for ORR applications has attracted a wealth of scientific interest for several decades [1–6].

Since cobalt phthalocyanine was observed to catalyze the ORR in 1964 [2], significant effort has been devoted to the synthesis of non-precious metal catalysts [3,7]. In particular, iron-based catalysts, synthesized by the pyrolysis of precursors composed of nitrogen, carbon and iron, have attracted extensive attention owing to their promising ORR activity. Previous studies have shown that the ORR activity of iron-based catalysts strongly depends on the synthesis procedure and the

* Corresponding author. Tel/Fax: +86-411-84379063; E-mail: sunshine@dicp.ac.cn
# Corresponding author. Tel/Fax: +86-411-84379063; E-mail: gqsun@dicp.ac.cn
This work was supported by the "Strategic Priority Research Program" of the Chinese Academy of Sciences (XDA09030104), the National Basic Research Program of China (973 Program, 2012CB215500), and the National Natural Science Foundation of China (21576258, 50823008).
DOI: 10.1016/S1872-2067(15)61049-X | http://www.sciencedirect.com/science/journal/18722067 | Chin. J. Catal., Vol. 37, No. 4, April 2016

precursor nature, which may influence the chemical states of iron and nitrogen heteroatoms and also the textural structure of the catalysts [8].

Conventional one-pot pyrolysis processes typically generate a low abundance of active sites, as when thermally activated Fe atoms are prone to agglomerate into large particles at high temperatures. To disperse iron uniformly in the host, various strategies, including ball-milling [3], wet-impregnation and ion exchange [9] have been extensively adopted. Recently, a spatial confinement strategy was proposed to synthesize various materials, including ultrafine metals and alloys where growth was restricted within two or three dimensional confined environments. The principal function is to confine the diffusion of atoms or the growth of particles to a limited space, thus producing unique characteristics in morphology, composition and/or microstructure [10,11].

Herein, we synthesized a Fe-N-C catalyst *via* a two-step pyrolysis process as illustrated in Scheme 1. The first step generates a nitrogen-doped carbon of high specific surface area (1227 $m^2/g$) by the pyrolysis of polypyrrole (PPy) and ethylenediaminetetraacetic acid disodium salt (EDTA-2Na). The second step uses the formed intermediate as a host to anchor iron producing a carbon matrix containing highly dispersed iron. The obtained Fe-N-C catalyst displays superior ORR activity in both alkaline and acid solutions. Furthermore, the methanol tolerance property of the Fe-N-C catalyst is critical in its advantage over the Pt/C catalyst for direct methanol fuel cells (DMFCs) as the Fe-N-C catalyst circumvents problems related to intractable methanol crossover. The DMFCs fabricated employing the Fe-N-C catalyst as the cathode display promising discharging performance.

## 2. Experimental

### 2.1. Synthesis of materials

The N-C catalyst was derived from PPy, which was obtained by polymerization of pyrrole. Briefly, 25 g cetyltrimethylammonium bromide (CTAB, $C_{19}H_{42}BrN$, Tianjin Guangfu Fine Chemical Research Institute) was dispersed in 80 mL ethylene glycol (EG, Tianjin Kemiou Chemical Reagent Co., Ltd.) followed by the addition of 6 mL pyrrole monomer ($C_4H_5N$, Sinopharm Chemical Reagent Co., Ltd.). After stirring for 1 h, 40 mL EG containing 12 g $FeCl_3·6H_2O$ was added dropwise with stirring. The polymerization process continued for 5 h before 200 mL methanol ($CH_3OH$, Xilong Chemical Co., Ltd.) was added and stirred overnight. The obtained black ink was then filtered, washed with water multiple times and dried in an oven at 80 °C for 8 h to obtain PPy. The obtained PPy was thermally treated under a $N_2$ atmosphere at 800 °C for 1 h to obtain the black powder, denoted as N-C.

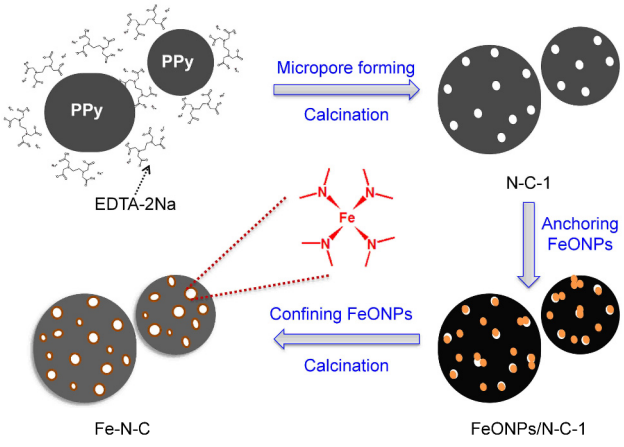


**Scheme 1.** Schematic diagram of the Fe-N-C catalyst synthesis route.

The above PPy was blended with EDTA-2Na ($C_{10}H_{14}N_2O_8Na_2·2H_2O$, Tianda Chemical Reagent Co., Ltd.) at a mass ratio of 1:2 in deionized water under vigorous stirring for 3 h, followed by evaporating the deionized water at 70 °C before drying at 80 °C. After grinding, the powder was thermally treated at 800 °C for 1 h under a $N_2$ atmosphere. Thereafter, the sample was sonicated in 1 mol/L HCl for ~2 h, washed with distilled water multiple times and dried in an oven at 80 °C overnight to obtain N-C-1.

$FeCl_3$ was hydrolyzed in an ethanol solution containing ammonia to obtain an iron oxide colloid (denoted as FeONPs), which was added to N-C-1 followed by thermal treatment to obtain the Fe-N-C sample. Briefly, a 0.2-mmol $FeCl_3$/ethanol solution and 2 mL 30% $NH_3·H_2O$ was added into 100 mL ethanol in a flask. The mixture was stirred and refluxed at 100 °C for 1 h. Subsequently, 200 mg N-C-1 was added and stirred for 4 h. Thereafter the solvent was evaporated using a rotary evaporator to obtain a black powder, which was then dried in an oven at 80 °C overnight. The obtained sample was pyrolyzed at 900 °C for 1 h under $N_2$ to obtain a loose and black powder, denoted as Fe-N-C.

N-C-2 was prepared for comparison with the Fe-N-C catalyst to discriminate the role of iron after the second thermal treatment. The N-C-1 was thermally treated in the absence of Fe at 900 °C for 1 h under a $N_2$ atmosphere.

### 2.2. Physical characterization

A scanning electron microscope (SEM, JSM-7800F) was used to study particle morphology, and energy-dispersive x-ray spectroscopy (EDX) was recorded on a specific area of the electrocatalyst. A transmission electron microscope (TEM, JEM-2100) was used to study the crystal nature of the electrocatalyst employing an acceleration voltage of 200 kV. The high resolution TEM (HRTEM) micrograph was obtained on a TEM (JEM-2100F) using an acceleration voltage of 200 kV. X-ray diffraction (XRD) studies were performed on a Rigaku X-2000 diffractometer using Cu $K_\alpha$ radiation with a Ni filter. The samples were scanned at a rate of 5°/min. The chemical composition of the four electrocatalysts were characterized by X-ray photoelectron spectroscopy (XPS) measurements (ESCALAB 250Xi) using Al $K_\alpha$ radiation.

Ar isotherms at −186 °C were measured using a Quantachrome Autosorb-iQ instrument. Before analysis, samples were outgassed at 180 °C under vacuum for 4 h. The Brunauer–Emmett–Teller (BET) surface area and pore size distribution was calculated by the non-linear density-functional theory

(NLDFT).

Room temperature $^{57}$Fe Mössbauer spectroscopy was used to investigate the oxidation state and coordination environment of iron ions in the Fe-N complexes. A $^{57}$Co (Rh) source, moving with a constant acceleration mode, was used as the γ-radiation source. The velocity was calibrated by a standard α-iron foil. The spectra were fitted with the appropriate Lorentzian line superpositions using the MossWinn 3.0i computer program. In this way, the $^{57}$Fe Mössbauer spectral parameters could be determined, including the isomer shift (IS), the electric quadrupole splitting (QS), the full width at half maximum, the hyperfine field ($H_{hf}$) and the relative resonance areas of the different components of the absorption patterns.

### 2.3. Electrochemical measurements

Rotating disk electrode (RDE) and rotating ring disc electrode (RRDE) measurements were conducted in a three-electrode cell setup with a computer-controlled bipotentiostat (Pine Company). The reference electrode was an Hg/HgO electrode (MMO) in 0.1 mol/L NaOH solution with respect to an alkaline electrolyte, and a standard calomel electrode (SCE) with a vacuum tube voltmeter for acidic electrolytes. The counter electrode was Pt wire. The MMO and SCE reference electrode were calibrated and the potential converted into reversible hydrogen electrode (RHE) in this study. To prepare the working electrode, 2.5 mg of catalyst powder was dispersed in 1 mL of ethanol and 25 μL of Nafion® solution (5 wt%, DuPont). The suspension was then sonicated for 15 min to form a homogeneous ink, thereafter, the ink was pipetted onto the surface of a glassy carbon disc (ø5.7 mm for RRDE and ø5.0 mm for RDE). The Fe-N-C loading was 0.62 mg/cm$^2$ and the Pt/C loading (20 wt% Pt/C, Johnson Matthey, JM) was 50 μg/cm$^2$.

For RRDE with the polycrystalline Pt biased at 1.23 V (vs. RHE), the working electrode surface was first electrochemically cleaned by cycling from 0.11–1.23 V (vs. RHE) for 20 cycles with a scan rate of 100 mV/s. The background cyclic voltammogram (CV) was then collected at a scan rate of 10 mV/s in a $N_2$-saturated 0.1 mol/L NaOH electrolyte. The RRDE measurement was performed in an $O_2$-saturated 0.1 mol/L NaOH electrolyte at a scan rate of 10 mV/s at 1600 r/min. The electron transfer number ($n$) is calculated according to Eq. (1).

$$n = 4I_d/(I_d+I_r/N) \quad (1)$$

where $I_r$ is the ring current, $I_d$ is the disc current, and $N$ is the collection efficiency for $H_2O_2$ by the RRDE (0.38) [12].

The accelerated aging test (AAT) was performed in an $O_2$-saturated 0.1 mol/L NaOH electrolyte scanning in the range of 0.60–1.00 V (vs. RHE) with a scan rate of 100 mV/s. The background CVs and the ORR polarization curves were recorded every 1000 potential cycles during the AAT.

With respect to an acidic electrolyte, the RDE measurements of Fe-N-C and 20 wt% Pt/C (JM) electrocatalysts were conducted from 0.10–1.20 V (vs. RHE) at a scan rate of 10 mV/s at 1600 r/min.

### 2.4. Fabrication of DMFCs and single cell tests

To obtain a membrane electrode assembly (MEA), the cathode and anode catalyst ink were painted directly on either side of the electrolyte membrane. The cathode was Fe-N-C or 20 wt% Pt/C (JM). The anode was PtRu black catalysts (JM). The catalyst inks were prepared by dispersing the catalyst into appropriate amounts of ethanol and a 5% Nafion® solution. A Nafion® 212 membrane (DuPont) and an anion-exchange membrane (Tokuyama) were used to fabricate acidic and alkaline DMFCs, respectively. The MEA and the diffusion carbon layers were hot pressed at 120 °C under a pressure of 500 pounds for 90 s. The active area of the MEA was 1 cm$^2$. The single cell was operated at 80 °C. The fuel used was 1 mol/L $CH_3OH$ at the flow rate of 1 mL/min for the acidic fuel cell, and 2 mol/L $CH_3OH$ in 1 mol/L NaOH at the flow rate of 2 mL/min for the alkaline fuel cell.

## 3. Results and discussion

To characterize the synthesis process of the Fe-N-C catalyst, the Ar adsorption-desorption isotherms of N-C, N-C-1, N-C-2, FeONPs/N-C-1 and Fe-N-C (Fig. 1(a)) were analyzed. The pore size distribution curves are depicted in Fig. 1(b), and the relevant data summarized in Table 1. For sample N-C-1, the isotherm presented a typical type-I behavior, with a steep increase

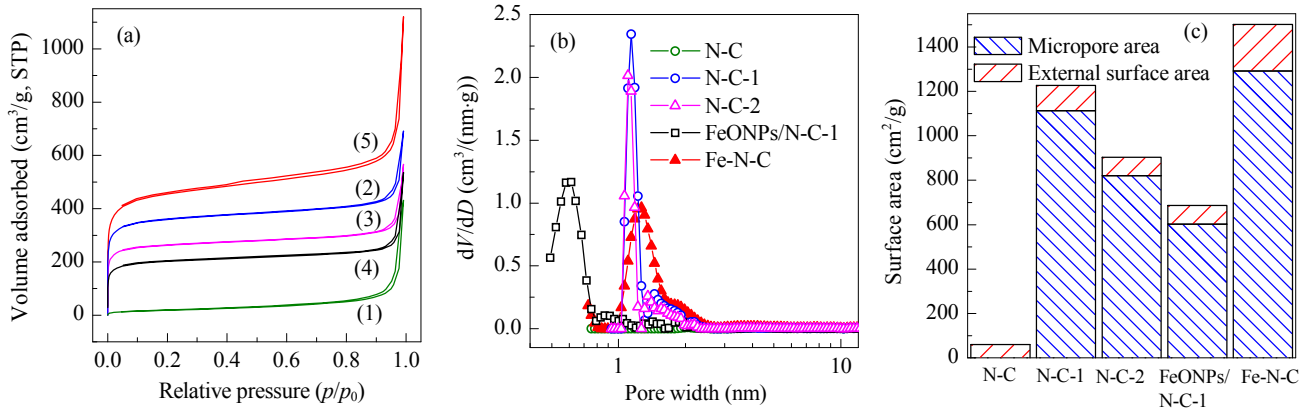


**Fig. 1.** (a) Ar adsorption-desorption isotherms, (b) the corresponding pore size distribution curves, and (c) the relative quantity of micropore area and external surface area for the electrocatalysts. (1) N-C; (2) N-C-1; (3) N-C-2; (4) FeONPs/N-C-1; (5) Fe-N-C.

**Table 1**
Electrocatalyst textural parameters characterized by Ar adsorption-desorption measurements.

| Catalyst | BET surface area ($m^2/g$) | Micropore surface area ($m^2/g$) | External surface area ($m^2/g$) | Pore width (nm) |
|---|---|---|---|---|
| N-C | 60 | 0 | 60 | 27 |
| N-C-1 | 1227 | 1113 | 113 | 1.1 |
| N-C-2 | 903 | 820 | 82 | 1.2 |
| FeONPs/N-C-1 | 687 | 603 | 83 | 0.6 |
| Fe-N-C | 1501 | 1292 | 209 | 1.3 |

of adsorbate uptake at low relative pressures. This suggested the presence of micropores. The specific surface area for N-C-1 was 1227 $m^2/g$ and the mean pore size was centered at 1.1 nm. In contrast, the sample N-C synthesized by directly pyrolyzing PPy showed an ultra low specific surface area (60 $m^2/g$) without obvious pore structure. As depicted in Fig. 1(c), the dramatic increase in specific surface area and the generation of micropores in N-C-1, as compared with N-C, benefitted from (1) the activation of carbon *via* $Na^+$ reacting with the carbon to generate Na and gaseous $CO_2$, and (2) the vast gaseous by-products from the precursors during the pyrolysis. However, for FeONPs/N-C-1, the specific surface area decreased significantly to 687 $m^2/g$ and the pore size decreased to 0.6 nm, indicating FeONPs dispersed on N-C-1 residing within or covering the micropores of N-C-1 as displayed in Scheme 1. After pyrolysis of FeONPs/N-C-1, the Fe-N-C sample possessed a significantly greater specific surface area (1501 $m^2/g$) and a slightly larger pore size (1.3 nm) over that of N-C-1 (Fig. 1(b)). However, for N-C-2 derived from N-C-1, although experiencing the same thermal treatment as that of the Fe-N-C, the specific surface area was only 903 $m^2/g$ and the pore size centered at 1.2 nm (Fig. 1(b)). Both textural properties were significantly

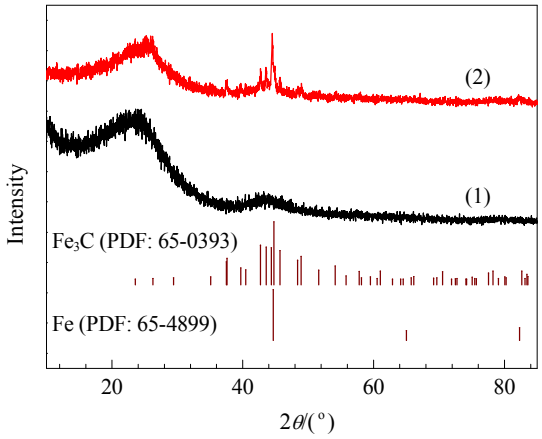


**Fig. 3.** XRD patterns of (1) N-C-2 and (2) Fe-N-C.

smaller than those of Fe-N-C, which suggested that FeONPs were confined by the micropores and further reacted with the active-edged nitrogen or carbon, thus enlarging the pore size, likely forming a new structure in the pores.

As shown in the SEM and TEM micrographs in Fig. 2, the Fe-N-C catalyst consisted of interconnected short carbon fibers averaging ~120 nm (Fig. 2(c, d)). Compared with the N-C-1 (Fig. 2(a, b)), the particles in Fe-N-C displayed no significant change. Although diffraction peaks assigned to Fe and $Fe_3C$ were detected in the XRD patterns of the Fe-N-C catalyst (Fig. 3), careful observation of the Fe-N-C sample by both low resolution (Fig. 2(e)) and HRTEM (Fig. 2(f)) found no metal or metal carbide/nitride crystals. The selected area electron diffraction (SAED) showed a diffraction ring (Fig. 2(e)), instead of separated diffraction spots, which suggested a poor crystal structure of the host carbon materials. Previous reports have

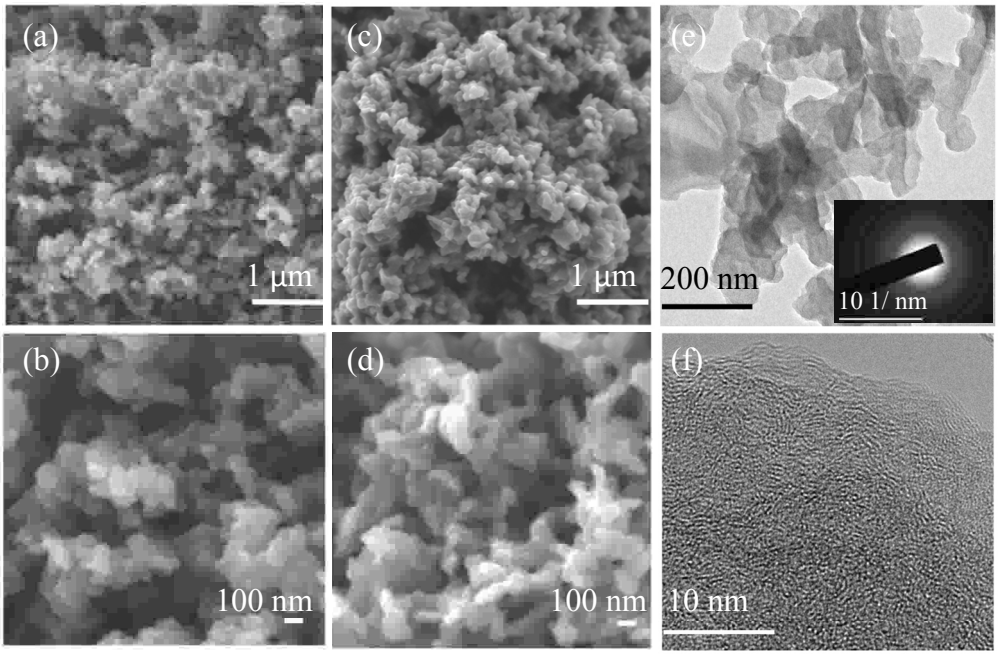


**Fig. 2.** SEM micrographs of N-C-1 (a, b), Fe-N-C (c, d) and TEM micrographs of Fe-N-C (e, f). The inset of (e) is the selected electron diffraction pattern of Fe-N-C.

also observed inconsistencies between XRD and TEM results in similar catalysts [13].

The scanning transmission electron microscope (STEM) elemental mapping micrographs further revealed that nitrogen and iron were homogeneously distributed across the entire carbon matrix (Fig. 4). Highly dispersed iron formation may be attributed to the following factors: (1) iron was well distributed in the FeONPs/N-C-1 precursor as confirmed by elemental mapping (Fig. 5), suggesting the anchoring effect of carbon micropores on iron; (2) during the pyrolysis of FeONPs/N-C-1, the nitrogen dopants and unsaturated carbon bonds protruding from the micropores confined the iron–nitrogen/carbon reaction to a limited space and inhibited the aggregation of iron.

The chemical state of nitrogen and iron in the carbon matrix was analyzed by XPS spectroscopy (Figs. 6, 7, 8(a), Tables 2 and 3). In general, for N-C, N-C-1, N-C-2 and Fe-N-C, carbon was dominant (82.2–87.8 at%). The nitrogen content varied from 4.9–7.2 at% in the four samples. Fe was detected only in sample Fe-N-C at 0.5 at%.

High resolution N 1*s* XPS spectra (Fig. 7(a)) were deconvoluted into five peaks according to a previous report [14], which were assigned to pyridinic-N (397.9–398.2 eV), pyrrole-N (400.6–400.8 eV), graphitic-N (401.8–402.1 eV), oxidized-N (403.1–403.5 eV) and nitrile-N for N-C type catalysts or Fe-$N_x$ for the Fe-N-C catalyst (399.3–399.7 eV) [15,16], respectively. Together with their respective concentrations, they are listed in Table 3. To compare clearly, the contents of nitrogen type are displayed in Fig. 7(b). Interestingly, for all these samples, the sum contents of pyridinic-N and graphitic-N, which are reported to be the most active N species for ORR, are similar (1.99–2.92 at%). Additionally, 0.77 at% N in the form of Fe-$N_x$

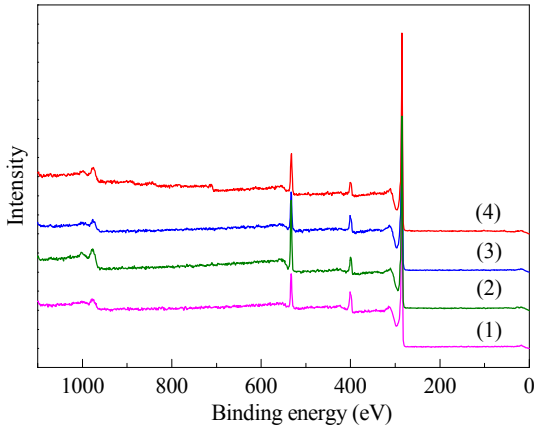


**Fig. 6.** XPS spectra of (1) N-C, (2) N-C-1, (3) N-C-2, and (4) Fe-N-C.

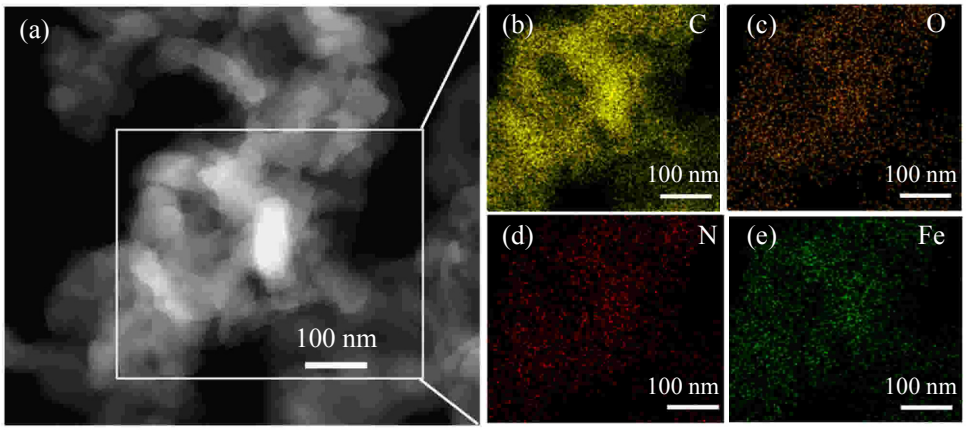


**Fig. 4.** (a) Scanning transmission electron microscope (STEM) micrograph of Fe-N-C and the corresponding elemental mapping of (b) carbon, (c) oxygen, (d) nitrogen, and (e) iron in a randomly selected region.

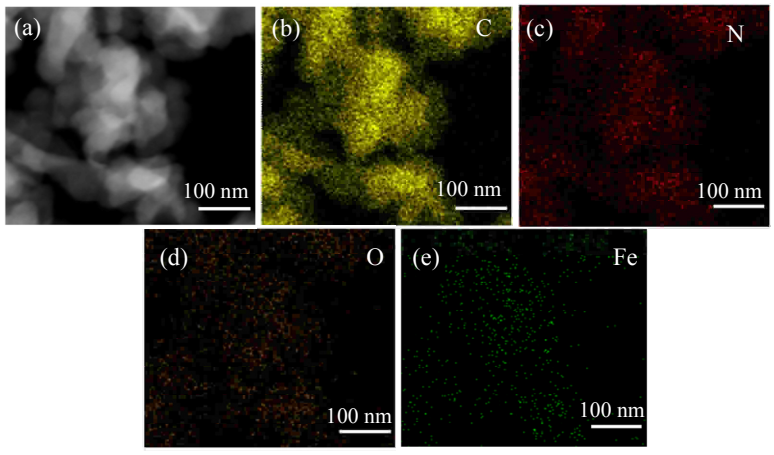


**Fig. 5.** (a) STEM micrograph of FeONPs/N-C-1 and the corresponding elemental mapping of (b) carbon, (c) nitrogen, (d) oxygen, and (e) iron in the selected region.

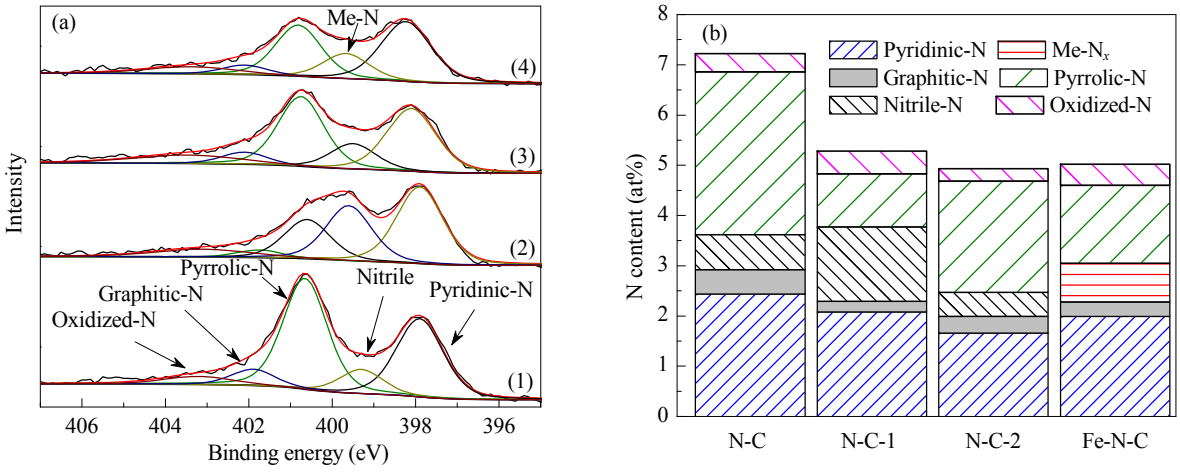


**Fig. 7.** (a) XPS spectra of N 1*s* and (b) the atomic percentage of nitrogen type in the electrocatalysts. (1) N-C; (2) N-C-1; (3) N-C-2; (4) Fe-N-C.

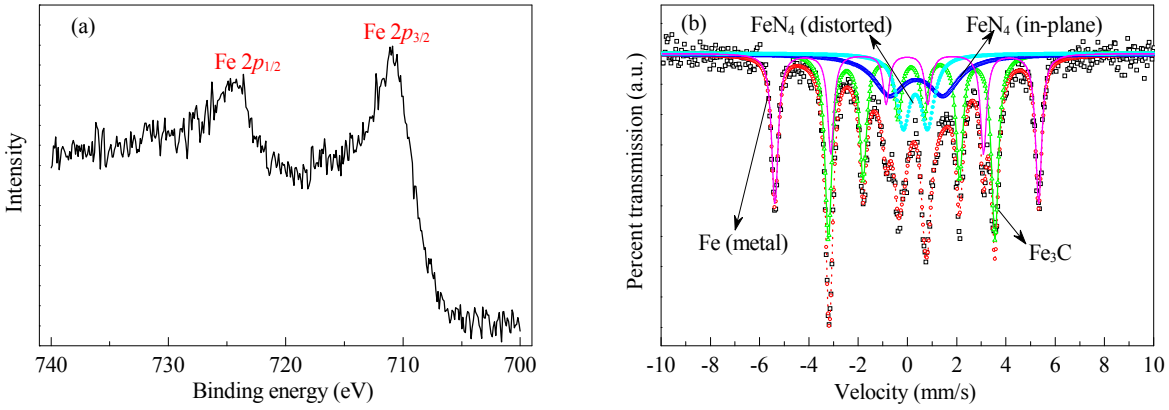


**Fig. 8.** (a) Fe 2*p* XPS spectrum and (b) Mössbauer spectra of Fe-N-C.

is contained in Fe-N-C.

In the high resolution Fe 2*p* XPS spectrum of Fe-N-C, the peaks at 711.0 and 724.3 eV (Fig. 8(a)) were assigned to Fe 2$p_{3/2}$ and Fe 2$p_{1/2}$, respectively, which corresponded to Fe(III) [16]. Thus, the iron at the surface of the Fe-N-C electrocatalyst may exist mainly in the form of a high oxidation state that coordinates with nitrogen. No signals for Fe (707 eV) and $Fe_3C$ (708 eV) appeared [17,18], further indicating that Fe and $Fe_3C$—present as characterized by XRD—may be enveloped in thick carbon layers.

Mössbauer spectroscopy is a technique based on the recoil-free absorption of γ rays by $^{57}Fe$ nuclei, and is effective in investigating the electron structure of iron coordination compounds. The Mössbauer spectra of Fe-N-C is depicted in Fig. 8(b), and the related parameters summarized in Table 4. In Fig. 8(b), the two doublets in blue and cyan are assigned to $FeN_4$ (in-plane) and $FeN_4$ (distorted), respectively [19]. These $FeN_4$ structures were believed to be at the catalyst surface, as the XPS also confirmed the presence of surface Fe-$N_x$ structures. The two sextets in green and magenta correspond to $Fe_3C$ and Fe (metal), respectively [19], which is consistent with the previous XRD analysis.

Combining the analysis results of TEM, XRD, XPS and the Mössbauer spectroscopy, it is clear that the Fe-N-C sample contained highly dispersed Fe-$N_4$ units, nitrogen-doped carbon and a relatively low concentration of large Fe and $Fe_3C$ particles. The Fe-$N_4$ units and the nitrogen-doped carbon were located at the surface, while Fe and $Fe_3C$ particles were likely to

**Table 2**
Sample elemental composition by XPS.

| Sample | C 1*s* | N 1*s* | O 1*s* | Fe 2*p* |
|---|---|---|---|---|
| N-C | 85.6 | 7.2 | 7.2 | — |
| N-C-1 | 82.2 | 5.3 | 12.6 | — |
| N-C-2 | 87.8 | 4.9 | 7.3 | — |
| Fe-N-C | 85.6 | 5.0 | 8.9 | 0.5 |

**Table 3**
Catalyst assignment of nitrogen type and respective atomic percentage.

| | | Pyridinic-N | Nitrile/Me-$N_x$ | Pyrrolic-N | Graphitic-N | Oxidized-N |
|---|---|---|---|---|---|---|
| N-C | B.E. (eV) | 397.9 | 399.3 | 400.7 | 401.9 | 403.2 |
| | Content (at%) | 2.44 | 0.70 | 3.24 | 0.48 | 0.36 |
| N-C-1 | B.E. (eV) | 397.9 | 399.6 | 400.6 | 401.8 | 403.1 |
| | Content (at%) | 2.08 | 1.48 | 1.06 | 0.21 | 0.45 |
| N-C-2 | B.E. (eV) | 398.1 | 399.5 | 400.8 | 402.1 | 403.5 |
| | Content (at%) | 1.66 | 0.48 | 2.21 | 0.33 | 0.25 |
| Fe-N-C | B.E. (eV) | 398.2 | 399.7 | 400.8 | 402.1 | 403.4 |
| | Content (at%) | 1.99 | 0.77 | 1.55 | 0.29 | 0.42 |

**Table 4**
Mössbauer parameter assignment linked to possible iron modifications.

| Sample | Component | IS (mm/s) | QS (mm/s) | $B_{hf}$ (T) | fwhm (mm/s) | Area (%) |
|---|---|---|---|---|---|---|
| Fe-N-C | Fe (Metal) | –0.02 | –0.01 | 33.3 | 0.30 | 28.3 |
| | $Fe_3C$ | 0.17 | 0.02 | 21.0 | 0.34 | 39.2 |
| | $FeN_4$ (in-plane) | 0.37 | 2.19 | — | 1.58 | 18.7 |
| | $FeN_4$ (distorted) | 0.33 | 0.99 | — | 0.64 | 13.9 |

IS: Isomer shift. QS: Quadrupole splitting. $B_{hf}$: Intensity of the internal magnetic field. fwhm: Full width at half maximum.

be beneath thick carbon layers because they were not detected by XPS.

The electrocatalytic activity was configured in the RRDE setup and performed in an oxygen-saturated 0.1-mol/L NaOH electrolyte with an electrode rotating rate of 1600 rpm (Fig. 9(a) and (b)). As depicted in Fig. 9(a), for the N-C catalyst synthesized directly by carbonizing PPy in the absence of EDTA-2Na, the onset potential ($E_0$) and the half wave potential ($E_{1/2}$) were ~0.87 and 0.64 V, respectively. $n$ varied in the range of 3.0–3.7, indicating a mixed two and four electron transfer process. For N-C-1, $E_0$ and $E_{1/2}$ shifted positively to 0.95 and 0.80 V, respectively, and $n$ varied in the range of 3.2–4.0, suggesting significant improved catalytic activity. $E_0$ and $E_{1/2}$ values relating to the ORR polarization curve for the Fe-N-C electrocatalyst were 1.08 and 0.88 V, respectively, which was similar to the values of the Pt/C catalyst (Fig. 9(c)). This demonstrated Fe-N-C possesses superior catalytic activity. $n$ for the Fe-N-C catalyst approached 4, with a hydrogen peroxide yield <3% (Fig. 9(b)), which suggested that oxygen was being electro-reduced to hydroxide *via* a four electron transfer process.

To understand the function of iron with respect to catalytic activity, the ORR polarization curves of the N-C-2 catalyst were also measured and compared (Fig. 9(a, b)). For N-C-2, although the catalyst was subjected to a second calcination process, similar to the Fe-N-C catalyst, not even a minor improvement in catalytic activity was observed compared with its precursor, N-C-1. Furthermore, the catalytic activity fell significantly short of the Fe-N-C catalyst (Fig. 9(a)), which implied the importance of iron for the ORR catalytic activity. Because $Fe_3C$ and Fe may have been beneath thick carbon layers, they could not directly participate in the catalytic process. Thus, the high catalytic activity of Fe-N-C was probably related to the surface $Fe-N_4$ structure based on the above XPS and Mössbauer spectra results. Additionally, the large surface area of the carbon host permitted considerable access of reagents to the active sites.

The durability of the Fe-N-C catalyst was tested *via* a standard accelerated aging procedure (see experimental section for details). The ORR polarization curves before and after the AAT presented a typical diffusion-controlled limiting current platform at large overpotentials (Fig. 9(c, d)). After 5000 continuous potential cycles, a negligible drop in the ORR current was

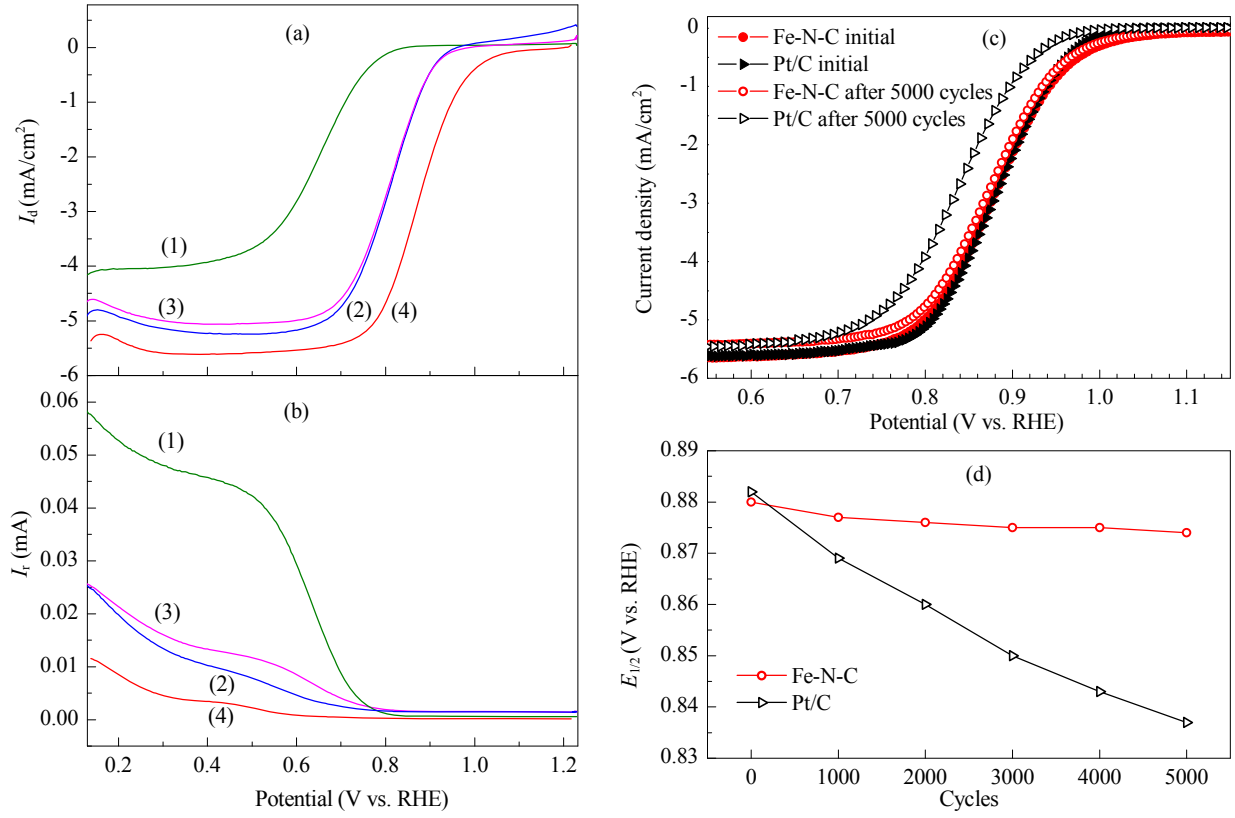


**Fig. 9.** ORR measurements of the electrocatalysts. (a) Disc currents; (b) Ring currents. Rotating ring disc electrode (RRDE) test conditions: $O_2$-saturated 0.1 mol/L NaOH, rotation rate 1600 r/min, scan rate 10 mV/s. (c) ORR polarization plots of the Fe-N-C (0.62 mg/cm$^2$) and Pt/C (50 μg/cm$^2$) electrocatalysts measured during 5000 cycles durability. (d) Half wave potential ($E_{1/2}$) of Fe-N-C and Pt/C at each 1000 cycles in the durability test. (1) N-C; (2) N-C-1; (3) N-C-2; (4) Fe-N-C.

observed for the Fe-N-C catalyst, while there was a 45-mV loss in $E_{1/2}$ for the Pt/C electrocatalyst under the same conditions (Fig. 9(c)). From the varying trends of the $E_{1/2}$ during the 5000 cycling procedure (Fig. 9(d)), it was clear that the ORR activity of Pt decreased linearly, while the Fe-N-C catalyst remained relatively stable. This suggests superior durability of the Fe-N-C catalyst over that of the Pt/C electrocatalyst in alkaline media.

Compared with Pt/C, the Fe-N-C catalyst is inert to methanol (Fig. 10(b)), a critical advantage for an effective cathodic catalyst for DMFCs [20]. The DMFC polarization curves with either Fe-N-C or a commercial Pt/C catalyst as the cathode are depicted in Fig. 10(c, d). In Fig. 10(c), with a proton exchange membrane, the maximum power density of the Fe-N-C cathode DMFC reaches up to 47 mW/cm², which is almost 60% of that for the Pt/C cathode DMFC (79 mW/cm²). In Fig. 10(d), with the anion-exchange membranes, the maximum power density of the Fe-N-C cathode DMFC is 33 mW/cm², while the Pt/C cathode DMFC only reaches to 8 mW/cm². There were some significant differences in the polarization curves between the Fe-N-C cathode DMFC and Pt/C cathode DMFC. (1) The open-circuit voltages (OCVs) of the Fe-N-C cathode DMFC were all higher than those with the Pt/C cathode irrespective of the media type. This was attributed to the excellent methanol tolerance property of Fe-N-C mitigating mixed potential at the cathode [21]. (2) In the electrochemical activation polarization region shown in Fig. 10(c, d), the Fe-N-C cathode DMFC performed better in alkaline media than in acidic media, which was consistent with the ORR activity of the Fe-N-C observed in the half cells (Fig. 9(a) and Fig. 10(a)). (3) In the high current density region, both Fe-N-C and Pt/C cathode DMFCs performed to a lower degree in alkaline media than in acidic media. This may indicate that the three-phase boundary required further optimization to tailor the alkaline fuel cells. However, the lower migration rate of hydroxyls when compared with protons may have degraded the performance in the high current density region. (4) In alkaline media, the polarization curve for the Pt/C cathode DMFC dropped to a greater extent than the Fe-N-C cathode DMFC. One reason is that for Pt/C, the methanol "crossing over" from the anode would be electro-oxidized at the cathode to produce $CO_2$, which combines with hydroxyl groups to generate carbonate salts. The local over-saturated concentration of the carbonate salts would form deposits, potentially blocking the electrode pores and impeding mass transport. This would in turn lead to the decreased per-

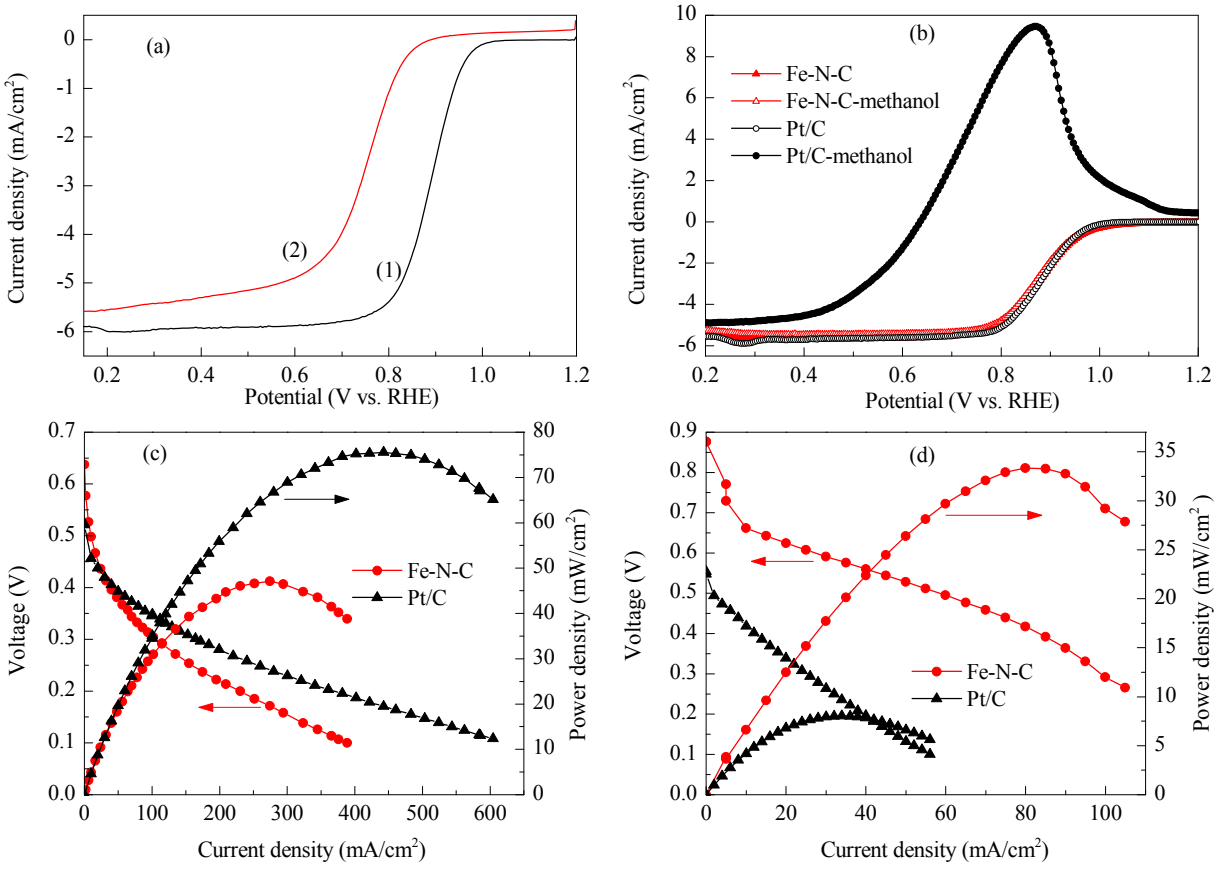


**Fig. 10.** (a) ORR polarization curves of (1) Pt/C and (2) Fe-N-C in $O_2$ saturated 0.1 mol/L $HClO_4$. (b) ORR polarization curves of Fe-N-C and Pt/C in $O_2$ saturated 0.1 mol/L NaOH in presence of methanol. (c) The acidic DMFC performance at 80 °C using Pt/C (0.16 mg Pt/cm²) or Fe-N-C (3.2 mg/cm²) as the cathode. The anode used was PtRu black (3.2 mg PtRu/cm²) with 1 mol/L $CH_3OH$ supplied at a flow rate of 1 mL/min. Dry oxygen was supplied to the cathode at flow rate of 100 mL/min. (d) The alkaline DMFC performance at 80 °C with Pt/C (0.12 mg Pt/cm²) or Fe-N-C (3.0 mg/cm²) used as the cathode. The anode used was PtRu black (3.0 mg PtRu/cm²) with 2 mol/L $CH_3OH$ in 1 mol/L NaOH supplied at a flow rate of 1 mL/min. Dry oxygen was supplied to the cathode at a flow rate of 100 mL/min.

formance of the Pt cathode DMFC. As for the Fe-N-C cathode, which has effective methanol tolerance, no carbonate salts would generate during the DMFC operation. The Fe-N-C cathode is therefore a promising alternative ORR catalyst over Pt in DMFC applications.

## 4. Conclusions

A Fe-N-C catalyst with iron uniformly dispersed in a carbon matrix possessing a high specific surface area (1501 $m^2/g$) was synthesized. The catalyst exhibited excellent ORR activity in both alkaline ($E_o$ = 1.08 V and $E_{1/2}$ = 0.88 V vs. RHE) and acid electrolytes ($E_o$ = 0.85 V and $E_{1/2}$ = 0.75 V vs. RHE). The detailed investigation on the composition–structure–performance relationship by XRD, XPS and Mössbauer spectroscopy suggests that Fe-$N_4$, graphitic-N and pyridinic-N are the active components for the ORR. The DMFC employing Fe-N-C as the cathodic catalyst displayed a maximum power density of 33 mW/$cm^2$ in alkaline media (vs. 8 mW/$cm^2$ for the Pt/C cathode DMFC) and 47 mW/$cm^2$ in acidic media (vs. 79 mW/$cm^2$ for the Pt/C cathode DMFC). The promising DMFC performance is attributed to both the superior ORR activity and the effectiveness of the Fe-N-C cathode to methanol tolerance.

## References


[1] M. K. Debe, *Nature*, **2012**, 486, 43–51.
[2] R. J. Jasinski, *Nature*, **1964**, 201, 1212–1213.
[3] M. Lefèvre, E. Proietti, F. Jaouen, J. P. Dodelet, *Science*, **2009**, 324, 71–74.
[4] K. P. Gong, F. Du, Z. H. Xia, M. Durstock, L. M. Dai, *Science*, **2009**, 323, 760–764.
[5] D. Banham, S. Ye, K. Pei, J. I. Ozaki, T. Kishimoto, Y. Imashiro, *J. Power Sources*, **2015**, 285, 334–348.
[6] Z. Yang, H. G. Nie, X. A. Chen, X. H. Chen, S. M. Huang, *J. Power Sources*, **2013**, 236, 238–249.
[7] G. Wu, K. L. More, C. M. Johnston, P. Zelenay, *Science*, **2011**, 332, 443–447.
[8] C. W. B. Bezerra, L. Zhang, K. Lee, H. Liu, A. L. B. Marques, E. P. Marques, H. Wang, J. Zhang, *Electrochim. Acta*, **2008**, 53, 4937–4951.
[9] J. Tian, A. Morozan, M. T. Sougrati, M. Lefèvre, R. Chenitz, J. P. Dodelet, D. Jones, F. Jaouen, *Angew. Chem. Int. Ed.*, **2013**, 125, 7005–7008.
[10] C. Baldizzone, S. Mezzavilla, H. W. P. Carvalho, J. C. Meier, A. K. Schuppert, M. Heggen, C. Galeano, J. D. Grunwaldt, F. Schüth, K. J. J. Mayrhofer, *Angew. Chem. Int. Ed.*, **2014**, 53, 1–6.
[11] C. Galeano, J. C. Meier, V. Peinecke, H. Bongard, I. Katsounaros, A. A. Topalov, A. Lu, K. J. J. Mayrhofer, F. Schuth, *J. Am. Chem. Soc.*, **2012**, 134, 20457–20465.
[12] J. Liu, L. H. Jiang, Q. W. Tang, B. S. Zhang, D. S. Su, S. L. Wang, G. Q. Sun, *ChemSusChem*, **2012**, 5, 2315–2318.
[13] Y. S. Zhu, B. S. Zhang, X. Liu, D. W. Wang, D. S. Su, *Angew. Chem. Int. Ed.*, **2014**, 53, 10673–10677.
[14] F. Jaouen, J. Herranz, M. Lefèvre, J. P. Dodelet, U. I. Kramm, I. Herrmann, P. Bogdanoff, J. Maruyama, T. Nagaoka, A. Garsuch, J. R. Dahn, T. Olson, S. Pylypenko, P. Atanassov, E. A. Ustinov, *ACS Appl. Mater. Interfaces*, **2009**, 1, 1623–1639.
[15] J. Zhang, D. P. He, H. Su, X. Chen, M. Pan, S. C. Mu, *J. Mater. Chem. A*, **2014**, 2, 1242–1246.
[16] Q. Cui, S. J. Chao, P. H. Wang, Z. Y. Bai, H. Y. Yan, K. Wang, L. Yang, *RSC Adv.*, **2014**, 4, 12168–12174.


### Graphical Abstract

*Chin. J. Catal.*, 2016, 37: 539–548 doi: 10.1016/S1872-2067(15)61049-X

**A Fe-N-C catalyst with highly dispersed iron in carbon for oxygen reduction reaction and its application in direct methanol fuel cells**

Lingzheng Gu, Luhua Jiang*, Xuning Li, Jutao Jin, Junhu Wang, Gongquan Sun*
*Dalian Institute of Chemical Physics, Chinese Academy of Sciences; University of Chinese Academy of Sciences*

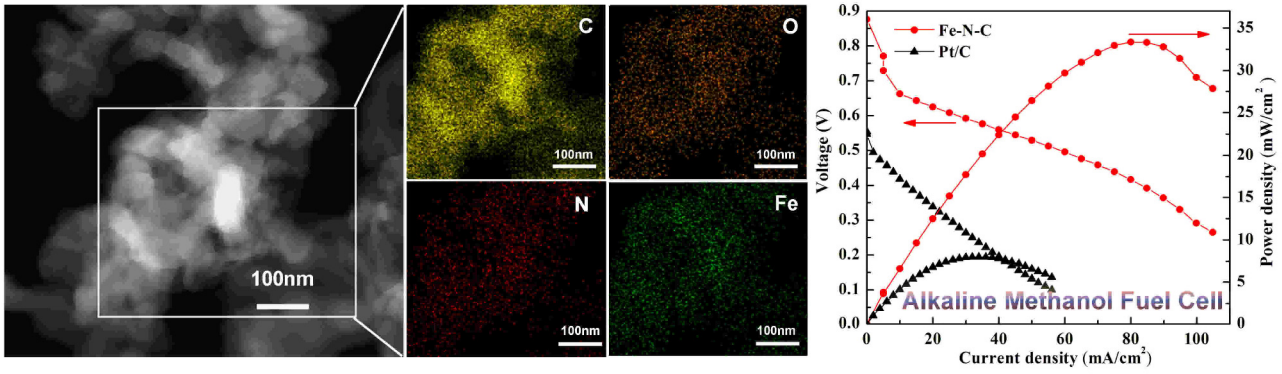


A highly dispersed Fe-N-C electrocatalyst, prepared *via* a two-step pyrolysis synthesis route, exhibits promising ORR activity. The Fe-N-C cathode DMFC possesses high catalytic activity together with excellent methanol tolerance properties and shows promising discharging performance.

[17] X. L. Dong, Z. D. Zhang, Q. F. Xiao, X. G. Zhao, Y. C. Chuang, S. R. Jin, W. M. Sun, Z. J. Li, Z. X. Zheng, H. Yang, *J. Mater. Sci.*, **1998**, 33, 1915–1919.
[18] J. S. Zhou, H. H. Song, X. H. Chen, L. J. Zhi, J. P. Huo, B. Cheng, *Chem. Mater.*, **2009**, 21, 3730–3737.
[19] U. I. Kramm, M. Lefèvre, N. Larouche, D. Schmeisser, J. P. Dodelet, *J. Am. Chem. Soc.*, **2013**, 136, 978–985.
[20] Y. Nie, L. Li, Z. D. Wei, *Chem. Soc. Rev.*, **2015**, 44, 2168–2201.
[21] M. L. Xiao, J. B. Zhu, L. G. Feng, C. P. Liu, W. Xing, *Adv. Mater.*, **2015**, 27, 2521–2527.